

MIT Open Access Articles

Constructing a Gapless Spin-Liquid State for the Spin-1/2 J_1 - J_2 Heisenberg Model on a Square Lattice

The MIT Faculty has made this article openly available. **Please share** how this access benefits you. Your story matters.

Citation: Wang, Ling, Didier Poilblanc, Zheng-Cheng Gu, Xiao-Gang Wen, and Frank Verstraete. "Constructing a Gapless Spin-Liquid State for the Spin-1/2 J_1 - J_2 Heisenberg Model on a Square Lattice." *Physical Review Letters* 111, no. 3 (July 2013). © 2013 American Physical Society

As Published: <http://dx.doi.org/10.1103/PhysRevLett.111.037202>

Publisher: American Physical Society

Persistent URL: <http://hdl.handle.net/1721.1/79916>

Version: Final published version: final published article, as it appeared in a journal, conference proceedings, or other formally published context

Terms of Use: Article is made available in accordance with the publisher's policy and may be subject to US copyright law. Please refer to the publisher's site for terms of use.



Constructing a Gapless Spin-Liquid State for the Spin-1/2 $J_1 - J_2$ Heisenberg Model on a Square Lattice

Ling Wang,^{1,2} Didier Poilblanc,³ Zheng-Cheng Gu,² Xiao-Gang Wen,^{4,5,6} and Frank Verstraete^{1,7}

¹Faculty of Physics, Vienna Center for Quantum Science and Technology, University of Vienna, Boltzmannngasse 5, 1090 Vienna, Austria

²Institute for Quantum Information and Matter, California Institute of Technology, Pasadena, California 91125, USA

³Laboratoire de Physique Théorique, C.N.R.S. and Université de Toulouse, 31062 Toulouse, France

⁴Perimeter Institute for Theoretical Physics, 31 Caroline Street North, Waterloo, Ontario N2L 2Y5, Canada

⁵Department of Physics, Massachusetts Institute of Technology, Cambridge, Massachusetts 02139, USA

⁶Institute for Advanced Study, Tsinghua University, Beijing 100084, People's Republic of China

⁷Faculty of Physics and Astronomy, University of Ghent, Krijgslaan 281 S9, B-9000 Ghent, Belgium
(Received 5 February 2013; revised manuscript received 25 June 2013; published 17 July 2013)

We construct a class of projected entangled pair states which is exactly the resonating valence bond wave functions endowed with both short range and long range valence bonds. With an energetically preferred resonating valence bond pattern, the wave function is simplified to live in a one-parameter variational space. We tune this variational parameter to minimize the energy for the frustrated spin-1/2 $J_1 - J_2$ antiferromagnetic Heisenberg model on the square lattice. Taking a cylindrical geometry, we are able to construct four topological sectors with an even or odd number of fluxes penetrating the cylinder and an even or odd number of spinons on the boundary. The energy splitting in different topological sectors is exponentially small with the cylinder perimeter. We find a power law decay of the dimer correlation function on a torus, and a $\ln L$ correction to the entanglement entropy, indicating a gapless spin-liquid phase at the optimum parameter.

DOI: [10.1103/PhysRevLett.111.037202](https://doi.org/10.1103/PhysRevLett.111.037202)

PACS numbers: 75.10.Kt, 75.10.Jm

Introduction.—Resonant valence bond (RVB) states, which were first proposed by Anderson [1] to describe a possible ground state for the $S = 1/2$ antiferromagnetic (AF) Heisenberg model on a triangular lattice, and later to explain the possible mechanism of high- T_c cuprates [2,3], provide us a rich tool box to construct the so-called spin-liquid states. The equal weight superposition of the nearest neighbor (NN) RVB state on square lattice was shown to be critical [4,5]. Several numerical works [6–9] have demonstrated that the equal weight NN RVB states on the kagome and triangular lattices are \mathbb{Z}_2 spin-liquid states. Recently, numerical breakthroughs claimed a spin-liquid ground state for the kagome Heisenberg model [10,11] and the frustrated spin-1/2 $J_1 - J_2$ AF Heisenberg model on the square lattice [12,13]. However, these works did not give direct access to the topological nature of the spin-liquid states; therefore, a simple variational wave function approach is highly desirable. Although the variational energy of the NN RVB state on the kagome lattice [7,9] is still higher than the energy obtained via the density matrix renormalization group method [10], the topological nature is well understood within the formalism of the projected entangled pair states (PEPSs) [7]. On the other hand, from a projective wave function [14] approach supplemented by a projective symmetry group analysis all possible spin-liquid states on the triangular [15], kagome [15–18], and honeycomb [19] lattices have been obtained and classified but, for all lattices, the energetically

favorable states are believed to involve longer range RVB. As a result, it is natural to think that a general RVB state within the PEPS formalism is a more practical variational wave function, where one can gain simultaneously an optimized energy and a comprehensive picture of the topological nature.

In this Letter, we introduce a general RVB state written as a $D = 3$ PEPS, different from Refs. [6,7]; i.e., it includes valence bonds of all lengths. With a properly chosen singlet sign convention that meets all lattice symmetries on the square lattice, we minimize the energy of the spin-1/2 $J_1 - J_2$ AF Heisenberg model at $J_2 = 0.5J_1$ against a single variational parameter c governing the decay amplitude of the long range valence bonds. The idea is therefore to introduce a simple yet competing wave function that enables us to fully understand the topological properties of the ground state of the frustrated magnets.

RVB states in PEPS formalism.—The equal weight superposition of the NN RVB states can be constructed using a PEPS with bond dimension $D = 3$ as follows: each physical site has four virtual spins attached, each of which spans a virtual dimension of spin $1/2 \oplus 0$. From the bond point of view, every pair of the NN virtual spins is projected to a block diagonal virtual spin singlet state:

$$|S\rangle = |01\rangle - |10\rangle + |22\rangle; \quad (1)$$

here the virtual indices “0, 1” span the subspace of spin 1/2 and virtual index “2” spans the subspace of spin 0.

At the physical site, a projector enforces one of the virtual spins with its spin-1/2 subspace to be mapped to the physical spin-1/2 state and the rest of virtual spins to stay in the spin 0 subspace, i.e., the 2 state:

$$\mathcal{P}_1 = \sum_{k=1}^4 (|\uparrow\rangle\langle 0|_k + |\downarrow\rangle\langle 1|_k) \otimes |222\rangle_{/k}; \quad (2)$$

here subscript “/k” stands for all except k. This PEPS, by contracting the virtual index of each \mathcal{S} at the bond and each \mathcal{P}_1 at the vertex, represents exactly the equal weight NN RVB states [20].

To allow long distance singlet pairings, we need spins to teleport: enforcing a singlet between sites i and j that are already paired in singlets (s_1, i) and (s_2, j) will generate a singlet pair (s_1, s_2) . The following projector realizes spin teleportation without increasing the bond dimension:

$$\mathcal{P}_2 = \sum_{i \neq j \neq k \neq l} (|\uparrow\rangle\langle 0|_i + |\downarrow\rangle\langle 1|_i) \otimes \langle 2|_j \otimes |\epsilon\rangle_{kl}; \quad (3)$$

here $|\epsilon\rangle_{kl} \equiv |01\rangle_{kl} - |10\rangle_{kl}$, and it forces spins connected via this site by bonds k and l into a singlet. A general RVB wave function is a parameter c weighted combination of projectors $\mathcal{P} \equiv \mathcal{P}_1 + c\mathcal{P}_2$ at each vertex $V \equiv \{v\}$ traced out with the bond singlets \mathcal{S} at each bond $B \equiv \{b\}$,

$$|\Psi\rangle_{\text{RVB}} = \prod_V \mathcal{P} \prod_B |\mathcal{S}\rangle. \quad (4)$$

The sign convention and symmetries.—Figures 1(a)–1(d) enumerates four possible \mathcal{P}_1 projectors and eight \mathcal{P}_2 projectors at each vertex. The bond singlet \mathcal{S} is chosen such that NN singlets point from sublattice A to B ; the corner singlets, which play the role of singlet teleportation, are oriented counter clockwise and preserve all lattice symmetries. The sign convention is demonstrated in Fig. 1(e).

The nearest NN singlet arises through two bond singlets and one corner singlet, as in Fig. 2(a). However, the weight of a diagonal singlet is comprised of two shortest paths of equal magnitude but opposite sign; thus, the net weight of the diagonal singlet is zero. The only shortest path to build the next range AB sublattice singlet is shown in Fig. 2(b),

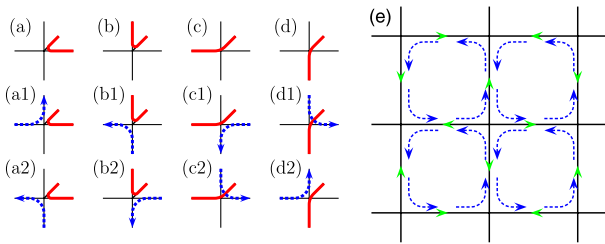


FIG. 1 (color online). (a)–(d) Red thick lines denote mappings of a virtual spin 1/2 to a physical spin 1/2, the blue dashed lines represent the singlet pairings of two virtual spin 1/2s, and the black thin lines represent the virtual spin 0 states. (e) The local sign convention for the bond singlets (in light green arrows) and the corner singlets (in dashed blue arrows).

and it consists of three bond singlets and two corners. The sign of the next range AB singlet is pointing from sublattice A to B . In general, no AA pairings survive [21] and all AB pairings point from sublattice A to B . To verify this result, we implement a Monte Carlo (MC) sampling of the singlet distribution of (3) and calculate the weight $h(dx, dy)$ defined in Ref. [14] as a function of separation. The result is presented in Fig. 2(c) and is consistent with the above analysis.

Variational ground state energies at $J_2 = 0.5J_1$.—We consider the general RVB wave function on a cylinder with finite cylindrical circumference N_v and infinite horizontal length $N_h = \infty$. The physical properties are determined by the eigenvector with the largest eigenvalue of the transfer matrix. Let us introduce a horizontal (vertical) parity number G_h (G_v) which is defined by counting the number of singlets modulo two that cross a horizontal (vertical) line joining the two boundaries of the cylinder (going around the cylinder). The two states with $G_h = \pm 1$ (+ is even and – is odd) are orthogonal to each other in the thermodynamic limit, and can be transformed from one to another by a cyclic spin permutation Π_{\circlearrowleft} operator winding around the cylinder as illustrated in Figs. 3(a) and 3(b).

The $G_h = \pm 1$ states are not the minimally entangled states [22]. However, their superpositions,

$$|\Psi(\pm)\rangle \equiv |\Psi\rangle_{G_h=1} \pm |\Psi\rangle_{G_h=-1}, \quad (5)$$

with a relative \pm sign are. A good reason for it is that these states (5) can be written as simple PEPSs: the $|\Psi(+)\rangle$ state is the state corresponding to Eq. (4), and $|\Psi(-)\rangle$ state is obtained by inserting a “vison” line to the PEPS for the state $|\Psi(+)\rangle$ as in Fig. 3(c). These minimally entangled states are referred to as the even-flux ($|\Psi(+)\rangle$) states and the odd-flux ($|\Psi(-)\rangle$) states which stand for the even and odd number of flux penetrating the cylinder. We will show next that these four states $|\Psi(\pm 1)\rangle_{e/o}$ are (bulk) ground

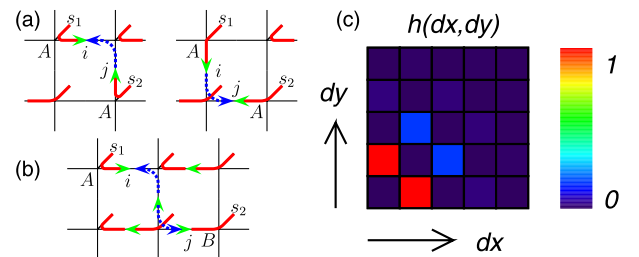


FIG. 2 (color online). (a) The nearest NN singlet (s_1, s_2) pairs through two bond singlets and one corner singlet via two paths, which cancel each other. (b) The next allowed AB sublattice pairing (s_1, s_2) through three bond singlets and two corner singlets. (c) The weight distribution in the Liang-Doucot-Anderson picture with a linear color scale for a 8×8 torus at $c = 0.35$. $h(dx, dy)$ is the weight of a singlet at separation (dx, dy) , where $h(1, 0) = 1$. The plotted color scale takes the square root of $h(dx, dy)$ to magnify the weight of the long range singlet.

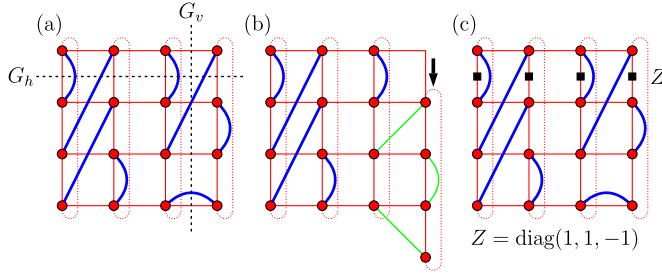


FIG. 3 (color online). (a) The parity quantum number G_v (G_h) is defined by counting the number of singlets (solid thick blue lines) modulo two crossed by a vertical loop (horizontal line) in dashed black line. (b) By cyclically permuting all spins in a loop winding around the cylinder, a $G_h = 1$ configuration in (a) is transformed into a $G_h = -1$ configuration in (b). Singlets in solid thin green lines are affected by the permutation operator. (c) An odd-flux state is defined by inserting operator Z on all vertical bonds crossed by a horizontal line to Eq. (3).

states of the gapless spin-liquid state, here the subscript e/o refers to the boundary quantum number G_v .

The variational energies of $|\Psi(\pm)\rangle_{e/o}$ on cylinders with finite perimeter $N_v = 4, 6, 8$ (N_v must be even, otherwise the system dimerizes) are computed *exactly* via the transfer matrix method and shown in Fig. 4(a) (an even or odd number of flux is chosen to provide the lowest energy) as a function of the variational parameter c . The best variational energy for the spin-1/2 $J_1 - J_2$ AF Heisenberg model at $J_2 = 0.5J_1$ is $c = 0.35(1)$ with $N_v = 4, 6, 8$. To access larger system size, we study a complementary geometry where the cylinders are cut open, with the top and bottom vertical virtual spins set to 2s. We call them the finite (N_v) width strips. For a contractible geometry as strips, the flux parity is no longer meaningful, but the boundary parity quantum number $G_v = e(o)$ still holds. We simulate the leading eigenvectors of the transfer matrix of the strips by the matrix product states with the same quantum number G_v in both bra and ket. The ground state energies as a function of the variational parameter c for both sectors

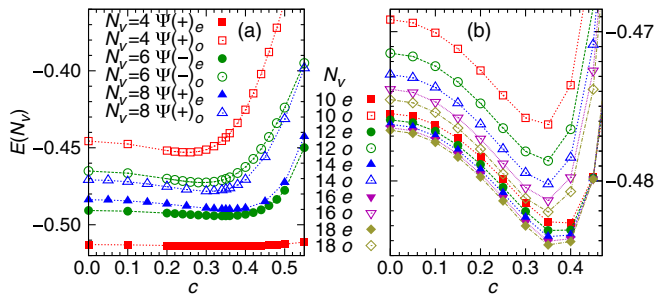


FIG. 4 (color online). Ground state energies (per site) computed for the $J_1 - J_2$ AF Heisenberg model at $J_2 = 0.5J_1$, as a function of parameter c for the e/o topological sectors of (a) a cylinder ($N_v = 4, 6, 8$) with even flux ($N_v/2$ even) or odd flux ($N_v/2$ odd), and (b) a strip geometry with $N_v = 10, \dots, 18$. For both cases, energy minimizes at $c = 0.35(1)$.

$(|\Psi\rangle_{e/o})$ of the strips with $N_v = 10, \dots, 18$ are presented in Fig. 4(b). The best variational energy for $J_2 = 0.5J_1$ is at $c = 0.35$, which is in good consistency with the case of finite perimeter cylinders.

The variational energies of the even and odd sectors at the optimum parameter $c = 0.35$ as a function of inverse width $1/N_v$ are shown in Figs. 5(a) and 5(b), with cylinders of size $N_v = 4, 6, 8$ and strips up to $N_v = 36$. A linear regression is applied to the even sector of the strips and a thermodynamic limit of $E_\infty = -0.48612(2)$ is obtained. This energy is competing on the third decimal digit to the best variational estimate of $E_\infty = -0.4943(7)$ with a $D = 9$ PEPS [13], let alone the fact that here we vary only one variational parameter in a $D = 3$ PEPS. A conjecture about the ground state energies of the gapless and gaped spin-liquid states is that the energy splittings between different topological sectors become exponentially small with the system size [23–25]. This conjecture is verified in Figs. 5(c) and 5(d), which present on semilog scales the energy difference between all sectors and E_∞ for cylinders and between the two existing energy sectors for strips.

Correlation functions and entanglement entropy.—We define the spin and dimer correlation functions as the ground state expectation values $C(r) = \langle S_0 \cdot S_r \rangle$ and $D^*(r) = \langle (S_0 \cdot S_1)(S_r \cdot S_{r+1}) - (S_0 \cdot S_1)(S_{r-1} \cdot S_r) \rangle$. Figure 6(a) plots the dimer correlation functions on a cylinder with $N_v = 8$ for all topological sectors at the optimal parameter $c = 0.35$. The odd sectors have very slowly decaying dimer correlations due to an odd number of spinons sitting on the boundaries; thus, the system effectively becomes an odd-width cylinder and the Majumdar-Ghosh-type of degeneracy emerges. We can

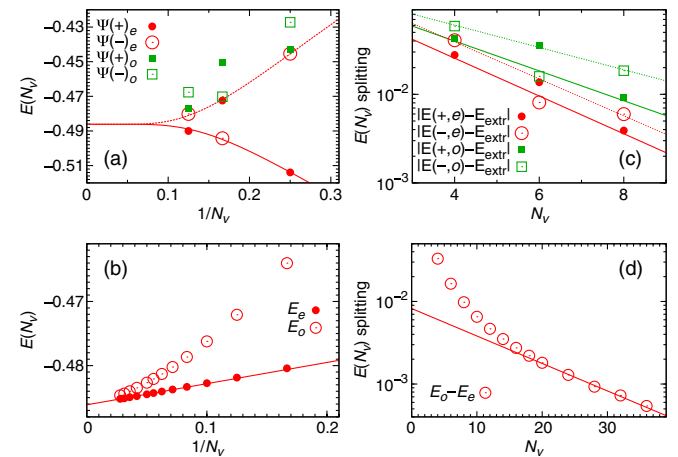


FIG. 5 (color online). Ground state energies at $c = 0.35$ as a function of $1/N_v$ for all topological sectors in (a) cylinders and (b) strips. The extrapolated ground state energy from the even sector of strips is $E_\infty = -0.48612(2)$. The ground state energy splitting between the lowest energy sector and other sectors as a function of N_v for (c) cylinders and (d) strips. The splitting vanishes exponentially with size N_v .

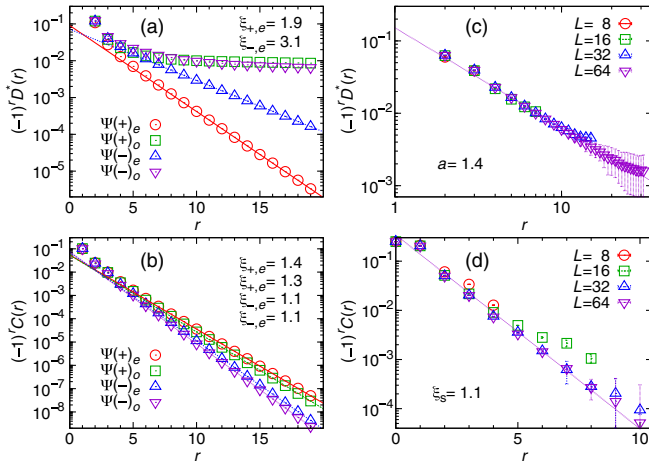


FIG. 6 (color online). The dimer (a) and the spin (b) correlation function for all topological sectors on a $N_v = 8$ cylinder at $c = 0.35$. The dimer (c) and the spin (d) correlation function on a torus with $L = 8, 16, 32, 64$ at $c = 0.35$. Note that different scales, log-log in (c) and semilog otherwise, are used.

eliminate the boundary effect by setting the system on a torus and carrying a variational MC simulation for PEPSs [26]. We found the dimer correlation function exhibits a power law decay $D^*(r) \sim ((-1)^r / r^a)$ with $a = 1.4$, as shown in Fig. 6(c). In contrast, the decay of the spin correlation function for all sectors on a cylinder or on a torus remains exponential with a correlation length $\xi_s \approx 1.1$, as evidenced in Figs. 6(b) and 6(d). Figure 7 shows the Renyi entropy $S_2(L)$ of an area $L \times L$ on a $2L \times L$ torus for size $L = 4, 6, \dots, 20$. The fitted line of $aL - (1/2) \ln L + b$ reflects the $\ln L$ correction from the oriented string picture [21]. The expected logarithmic correction has been discussed in other well-known gapless systems [27–29]. The simulation is done via MC sampling of the RVB configuration [30]. Finally, we also would like to point out that the logarithmic correction is very hard to be detected on a small system size. If we fit S_2 with a form $aL + b$ on a small system size, we find that the constant $b = -0.68(1)$, which is very close to $-\ln 2$. Such an observation implies that the observed $-\ln 2$ constant in the density matrix renormalization group calculation [12] is insufficient to rule out the possibility of a gapless spin-liquid ground state for the $J_1 - J_2$ Heisenberg model on a square lattice.

Conclusion and outlook.—We constructed a class of projected entangled pair states which exactly represent general RVB wave functions with all bond length contributions. Upon choosing an energetically preferred RVB pattern, we are able to build a one-parameter manifold of variational RVB $D = 3$ PEPSs which preserve all lattice symmetries. Minimization of the variational energy for the frustrated spin-1/2 $J_1 - J_2$ AF Heisenberg model on the square lattice yields, at $J_2 = 0.5J_1$, an energy $E_\infty = -0.48612(2)$ per site in the thermodynamic limit. In the case of a cylinder geometry, four orthogonal topological

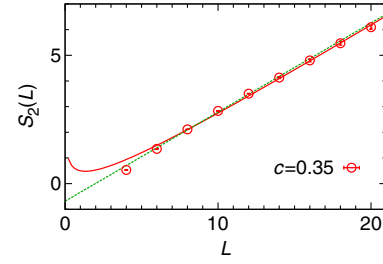


FIG. 7 (color online). Renyi entanglement entropy $S_2(L)$ for an area $L \times L$ on a torus of size $2L \times L$ with $L = 4, \dots, 20$. The fitted solid red line is of form $S_2(L) = a_1 L - (1/2) \ln L + b_1$ for $L \in [6:20]$; the fitted dashed green line is $S_2(L) = a_2 L + b_2$ for $L \in [6:14]$ and $b_2 = -0.68(1)$.

states were identified, namely, the even-flux and odd-flux states with an even and odd number of spinons on the boundary. We found the dimer correlation function decays algebraically while the spin correlation function still decays exponentially. The entanglement entropy scaling reveals the $\ln L$ correction to the area law. Both features point toward the gapless spin-liquid nature of our constructed RVB wave function.

The PEPSs construction of the general RVB states can be applied to other bipartite and nonbipartite lattices, where the Schwinger boson spin-liquid states under the projective symmetry group analysis have been found [15–19,31], but for which thermodynamic energies and correlation functions are still unknown due to a negative sign problem in the valence bond MC simulations. Within the PEPS formalism all of these can be easily studied. Our PEPS construction of the RVB states can be further generalized to accommodate a more complicated pairing pattern which can improve further the ground state energy, although it would possibly require a larger bond dimension.

We would also like to thank N. Schuch, I. Cirac, D. Perez-Garcia, and O. Motrunich for stimulating discussions. This project is supported by the EU Strep project QUEVADIS, the ERC grant QUERG, the FWF SFB grants FoQuS and ViCoM, and the NQTP ANR-0406-01 grant (French Research Council). X. G. W. is supported by NSF Grants No. DMR-1005541, No. NSFC 11074140, and No. NSFC 11274192. Research at Perimeter Institute is supported by the Government of Canada through Industry Canada and by the Province of Ontario through the Ministry of Research. The computational results presented have been achieved using the Vienna Scientific Cluster (VSC) and the CALMIP Hyperion Cluster (Toulouse).

- [1] P. W. Anderson, *Mater. Res. Bull.* **8**, 153 (1973).
- [2] P. W. Anderson, *Science* **235**, 1196 (1987).
- [3] P. A. Lee, N. Nagaosa, and X.-G. Wen, *Rev. Mod. Phys.* **78**, 17 (2006).

- [4] A. F. Albuquerque and F. Alet, *Phys. Rev. B* **82**, 180408 (R) (2010).
- [5] Y. Tang, A. W. Sandvik, and C. L. Henley, *Phys. Rev. B* **84**, 174427 (2011).
- [6] N. Schuch, D. Poilblanc, J. I. Cirac, and D. Perez-Garcia, *Phys. Rev. B* **86**, 115108 (2012).
- [7] D. Poilblanc, N. Schuch, D. Perez-Garcia, and J. I. Cirac, *Phys. Rev. B* **86**, 014404 (2012).
- [8] J. Wildeboer and A. Seidel, *Phys. Rev. Lett.* **109**, 147208 (2012).
- [9] F. Yang and H. Yao, *Phys. Rev. Lett.* **109**, 147209 (2012).
- [10] S. Yan, D. A. Huse, and S. R. White, *Science* **332**, 1173 (2011).
- [11] S. Depenbrock, I. P. McCulloch, and U. Schollwöck, *Phys. Rev. Lett.* **109**, 067201 (2012).
- [12] H.-C. Jiang, H. Yao, and L. Balents, *Phys. Rev. B* **86**, 024424 (2012).
- [13] L. Wang, Z.-C. Gu, F. Verstraete, and X.-G. Wen, [arXiv:1112.3331](https://arxiv.org/abs/1112.3331).
- [14] S. Liang, B. Douçot, and P. W. Anderson, *Phys. Rev. Lett.* **61**, 365 (1988).
- [15] F. Wang and A. Vishwanath, *Phys. Rev. B* **74**, 174423 (2006).
- [16] Y. Ran, M. Hermele, P. A. Lee, and X.-G. Wen, *Phys. Rev. Lett.* **98**, 117205 (2007).
- [17] T. Tay and O. I. Motrunich, *Phys. Rev. B* **84**, 020404(R) (2011).
- [18] T. Tay and O. I. Motrunich, *Phys. Rev. B* **84**, 193102 (2011).
- [19] F. Wang, *Phys. Rev. B* **82**, 024419 (2010).
- [20] F. Verstraete, M. M. Wolf, D. Perez-Garcia, and J. I. Cirac, *Phys. Rev. Lett.* **96**, 220601 (2006).
- [21] In the supplemental material, we showed that the RVB wave function has no same lattice pairings; we present an oriented string picture to rationalize the logarithmic correction to the entanglement entropy; this correction is further evidenced by the results from entanglement spectra and boundary Hamiltonian; finally, we provide the finite size scaling to establish the best variational parameter c and the variational ground state energy in the thermodynamic limit. See Supplemental Material at <http://link.aps.org/supplemental/10.1103/PhysRevLett.111.037202>.
- [22] Y. Zhang, T. Grover, A. Turner, M. Oshikawa, and A. Vishwanath, *Phys. Rev. B* **85**, 235151 (2012).
- [23] X. G. Wen and Q. Niu, *Phys. Rev. B* **41**, 9377 (1990).
- [24] X. G. Wen, *Int. J. Mod. Phys. B* **05**, 1641 (1991).
- [25] D. Poilblanc and N. Schuch, *Phys. Rev. B* **87**, 140407 (2013).
- [26] L. Wang, I. Pizorn, and F. Verstraete, *Phys. Rev. B* **83**, 134421 (2011).
- [27] A. B. Kallin, M. B. Hastings, R. G. Melko, and R. R. P. Singh, *Phys. Rev. B* **84**, 165134 (2011).
- [28] H. Ju, A. B. Kallin, P. Fendley, M. B. Hastings, and R. G. Melko, *Phys. Rev. B* **85**, 165121 (2012).
- [29] J. M. Stéphan, H. Ju, P. Fendley, and R. G. Melko, *New J. Phys.* **15**, 015004 (2013).
- [30] M. B. Hastings, I. Gonzalez, A. B. Kallin, and R. G. Melko, *Phys. Rev. Lett.* **104**, 157201 (2010).
- [31] T. Li, F. Becca, W. Hu, and S. Sorella, *Phys. Rev. B* **86**, 075111 (2012).